

An Effective Multigrid Method for High-Speed Flows

R. C. Swanson
NASA Langley Research Center
Hampton, VA 23665

E. Turkel *
Tel-Aviv University
Tel-Aviv 69978, Israel
and
Institute for Computer Applications in Science and Engineering
Hampton, VA 23665

J. A. White
Analytical Services and Materials, Inc.
Hampton, VA 23665

Abstract

We consider the use of a multigrid method with central differencing to solve the Navier-Stokes equations for high-speed flows. The time-dependent form of the equations is integrated with a Runge-Kutta scheme accelerated by local time stepping and variable coefficient implicit residual smoothing. Of particular importance are the details of the numerical dissipation formulation, especially the switch between the second and fourth difference terms. Solutions are given for two-dimensional laminar flow over a circular cylinder and a 15 degree compression ramp.

*This research was partially supported by the National Aeronautics and Space Administration under NASA Contract No. NAS1-18605 while the second author was in residence at the Institute for Computer Applications in Science and Engineering (ICASE), NASA Langley Research Center, Hampton, VA 23665.



Introduction

During the 1980's a wide variety of numerical schemes were investigated for solving the Euler and Navier-Stokes equations. Multistage time-stepping schemes with central differencing and multigrid acceleration [1, 2, 3] were demonstrated to be quite effective in computing subsonic and transonic flows over aerodynamic components and configurations. With the recent resurgence of interest in high-speed flight vehicles, we now need to construct versatile algorithms for hypersonic flow. One must keep in mind that hypersonic flows represent a formidable challenge for any flow solver. In particular, strong shock and expansion waves can occur in the flow field, and they can interact with each other and with shear layers (i.e., boundary layers, jets, wakes). Such strong nonlinear behavior and interactions can easily cause divergence of any numerical integration procedure. This is especially true during the initial phase of a calculation with a time-dependent method. So even the most successful algorithms of the last decade may require significant modifications to be effective for hypersonic flows.

An initial effort [4] to apply a central-difference multigrid algorithm to high-speed flows resulted in numerical difficulties that prevented the calculation of two-dimensional flows (i.e., blunt body and wedge type) with a Mach number higher than about 7. In order to compute such flows a low Courant-Friedrichs-Lewy (CFL) number was required. Thus four and five stage schemes were not practical, since there is substantial deterioration in the high frequency damping of the scheme due to the large reduction in the CFL number. The CFL restriction reduced the potential of the scheme as a viscous flow solver. More recently an algorithm utilizing a semicoarsening technique, a symmetric TVD formulation, and a three stage Runge-Kutta scheme [5] was proposed and used to compute high Reynolds number (laminar) Mach 10 flow over an airfoil at 10 degrees angle of attack. A good resolution of the bow shock wave and a reasonable convergence rate were obtained. The method of semicoarsening considered required a much more complicated cycle strategy than that employed with standard multigrid methods. In addition, it appears to be somewhat cumbersome to implement in three dimensions.

It is our contention that standard multigrid techniques can be used in conjunction with central differencing to compute hypersonic flows effectively. To achieve such success with these techniques one needs to give appropriate attention to both the advection and the dissipative processes of hyperbolic multigrid. The advection process provides a mechanism by which long wave disturbances can be rapidly expelled. In a multigrid method with a time-dependent iterative procedure, efficiency is in part derived from the larger time steps allowed on coarser meshes. Hence, it is important that the driving scheme of the multigrid method use large time steps. The dissipative process is essential in smoothing short wave disturbances. With this process the multigrid efficiency is based on principles similar to that for elliptic equations.

For hypersonic flows one encounters an additional consideration regarding the damping of the short waves. As the Mach number increases the jumps across shocks become larger, and it becomes more difficult to eliminate these high frequency oscillations. Thus a considerable part of the following discussion will concentrate on the smoothing algorithm. The fundamental features of the multigrid process (i.e., Full Approximation Storage scheme, grid transfer operators, fixed cycle strategy) are fairly standard. Other aspects, such as type of coarse grid correction scheme and procedure for smoothing of coarse grid corrections, found crucial in the present work will be emphasized. In this paper we consider a Runge-Kutta scheme [6] as the smoother for the multigrid method.

Central differences for spatial approximations are augmented by an artificial viscosity based on TVD principles [7]. Several changes are made to the numerical algorithm so that a converged solution can be obtained for high-speed flows. We initially describe the Runge-Kutta method for the central-difference scheme with numerical viscosity. We finally present some examples to demonstrate our conclusions.

Basic Scheme

The basic elements of the scalar dissipation model considered in this paper were first introduced by Jameson, Schmidt, and Turkel [6] in conjunction with Runge-Kutta explicit schemes. The spatial discretization is based on central differences with an additional artificial viscosity. This algorithm has been used by many investigators to solve the Euler equations numerically for a wide range of fluid dynamic applications. The same type of spatial discretization has been applied to alternating direction implicit (ADI) schemes [8] and LU factored implicit schemes [9]. In this section the basic scheme is briefly reviewed.

Consider the Euler equations in the form

$$W_t + f_x + g_y = 0, \quad (1)$$

where the four-component vector of conserved variables

$$W = [\rho \quad \rho u \quad \rho v \quad \rho E]^T, \quad (2)$$

and f, g are the corresponding flux vectors. The quantity ρ is the density, u and v are the Cartesian velocity components, and E is the specific total internal energy. The independent variables are time t and Cartesian coordinates (x, y) . If (1) is transformed to arbitrary curvilinear coordinates $\xi = \xi(x, y)$ and $\eta = \eta(x, y)$, then we obtain

$$(J^{-1}W)_t + F_\xi + G_\eta = 0, \quad (3)$$

where J^{-1} is the inverse transformation Jacobian, and

$$F = fy_\eta - gx_\eta, \quad G = gx_\xi - fy_\xi.$$

In a cell-centered, finite-volume method, (1) is integrated over an elemental volume in the discretized computational domain, and J^{-1} is identified as the volume of the cell. Equation (3) can also be written as

$$J^{-1}W_t + AW_\xi + BW_\eta = 0,$$

where A and B are the flux Jacobian matrices defined by $A = \partial F / \partial W$ and $B = \partial G / \partial W$.

To advance the scheme in time we use a multistage scheme. A typical step of a Runge-Kutta approximation to (3) is

$$W^{(k)} = W^{(0)} - \alpha_k \frac{\Delta t}{J^{-1}} [D_\xi F^{(k-1)} + D_\eta G^{(k-1)} - AD], \quad (4)$$

where D_ξ and D_η are spatial differencing operators, and AD represents the artificial dissipation terms. The derivatives of the fluxes are approximated by central differences.

The dissipation terms are a blending of second and fourth differences. That is,

$$AD = (D_\xi^2 + D_\eta^2 - D_\xi^4 - D_\eta^4) W, \quad (5)$$

where

$$D_\xi^2 W = \nabla_\xi \left[\left(\lambda_{\xi_{i+\frac{1}{2},j}} \epsilon_{i+\frac{1}{2},j}^{(2)} \right) \Delta_\xi \right] W_{i,j}, \quad (6)$$

$$D_\xi^4 W = \nabla_\xi \left[\left(\lambda_{\xi_{i+\frac{1}{2},j}} \epsilon_{i+\frac{1}{2},j}^{(4)} \right) \Delta_\xi \nabla_\xi \Delta_\xi \right] W_{i,j}, \quad (7)$$

and Δ_ξ , ∇_ξ are the standard forward and backward difference operators, respectively, associated with the ξ direction. The variable scaling factor λ is chosen as

$$\lambda_{\xi_{i+\frac{1}{2},j}} = \frac{1}{2} \left[(\lambda_\xi)_{i,j} + (\lambda_\xi)_{i+1,j} \right], \quad (8)$$

where λ_ξ is proportional to the spectral radius of the matrix A . The coefficients $\epsilon^{(2)}$ and $\epsilon^{(4)}$ are adapted to the flow and are defined as follows:

$$\epsilon_{i+\frac{1}{2},j}^{(2)} = \kappa^{(2)} \max(\nu_{i-1,j}, \nu_{i,j}, \nu_{i+1,j}, \nu_{i+2,j}), \quad (9)$$

$$\nu_{i,j} = \frac{|p_{i+1,j} - 2p_{i,j} + p_{i-1,j}|}{p_{i+1,j} + 2p_{i,j} + p_{i-1,j}}, \quad (10)$$

$$\epsilon_{i+\frac{1}{2},j}^{(4)} = \max \left[0, \left(\kappa^{(4)} - \epsilon_{i+\frac{1}{2},j}^{(2)} \right) \right], \quad (11)$$

where p is the pressure, and the quantities $\kappa^{(2)}$ and $\kappa^{(4)}$ are constants to be specified. The operators for the η direction are defined in a similar manner.

In this paper we will also consider a matrix form of the dissipation model just described. The model of (5)-(11) is characterized as a scalar formulation, since the dissipation for each discrete conservation equation is scaled by the same eigenvalue. As discussed in [7], a matrix form is obtained by replacing λ with a matrix, so that each equation will be scaled by its corresponding eigenvalue. That is, in the ξ direction, the $|A|$ is substituted for the eigenvalue scaling factor, λ , in (6) and (7). For the η direction, ξ and $|A|$ are replaced by η and $|B|$, respectively. A convenient form for the matrix $|A|$ is defined in the following way. Let

$$\Lambda = \text{Diag} [\lambda_1 \ \lambda_2 \ \lambda_3 \ \lambda_3]$$

with

$$\begin{aligned} \lambda_1 &= q + \sqrt{a_1^2 + a_2^2} \ c, & \lambda_2 &= q - \sqrt{a_1^2 + a_2^2} \ c, & \lambda_3 &= q, \\ a_1 &= J^{-1} \xi_x, & a_2 &= J^{-1} \xi_y, & q &= a_1 u + a_2 v. \end{aligned}$$

and c representing the speed of sound. Then,

$$\begin{aligned} |A| &= |\lambda_3| I + \left(\frac{|\lambda_1| + |\lambda_2|}{2} - |\lambda_3| \right) \left[\frac{\gamma - 1}{c^2} E_1 + \frac{1}{a_1^2 + a_2^2} E_2 \right] \\ &+ \frac{|\lambda_1| - |\lambda_2|}{2} \left(\frac{1}{\sqrt{a_1^2 + a_2^2} \ c} \right) [E_3 + (\gamma - 1) E_4], \end{aligned} \quad (12)$$

where

$$E_1 = \begin{bmatrix} \phi & -u & -v & 1 \\ u\phi & -u^2 & -uv & u \\ v\phi & -uv & -v^2 & v \\ H\phi & -uH & -vH & H \end{bmatrix},$$

$$E_2 = \begin{bmatrix} 0 & 0 & 0 & 0 \\ -a_1q & a_1^2 & a_1a_2 & 0 \\ -a_2q & a_2a_1 & a_2^2 & 0 \\ -q^2 & qa_1 & qa_2 & 0 \end{bmatrix},$$

$$E_3 = \begin{bmatrix} -q & a_1 & a_2 & 0 \\ -uq & ua_1 & ua_2 & 0 \\ -vq & va_1 & va_2 & 0 \\ -Hq & Ha_1 & Ha_2 & 0 \end{bmatrix},$$

$$E_4 = \begin{bmatrix} 0 & 0 & 0 & 0 \\ a_1\phi & -a_1u & -a_1v & a_1 \\ a_2\phi & -a_2u & -a_2v & a_2 \\ q\phi & -qu & -qv & q \end{bmatrix},$$

H is the total enthalpy, and $\phi = (u^2 + v^2)/2$. Notice the special form of $|A|$, where each row of E_j is either a scalar times the first row or a scalar times the second row when the first row contains only zeros. Due to this special form for any λ_1 , λ_2 , and λ_3 , an arbitrary vector x can be multiplied by $|A|$ very quickly. That is, one calculates $|A_{j+\frac{1}{2}}|(u_{j+1} - u_j)$ directly, rather than calculate $|A_{j+\frac{1}{2}}|$ and multiply a matrix times a vector. The matrix $|B|$ is computed in the same way as $|A|$ by simply replacing ξ with η .

In practice one cannot choose $\lambda_1, \lambda_2, \lambda_3$ as given above. Near stagnation points λ_3 approaches zero while near sonic lines λ_1 or λ_2 approach zero. A zero artificial viscosity would create numerical difficulties. To prevent such problems, these values are limited as

$$|\tilde{\lambda}_1| = \max(|\lambda_1|, V_n \rho(A)), \quad \rho(A) = |q| + c\sqrt{a_1^2 + a_2^2}, \quad (13)$$

$$|\tilde{\lambda}_2| = \max(|\lambda_2|, V_n \rho(A)), \quad |\tilde{\lambda}_3| = \max(|\lambda_3|, V_\ell \rho(A)), \quad (14)$$

where the linear eigenvalue λ_3 can be limited differently than the nonlinear eigenvalues. The parameters V_n and V_ℓ are determined numerically, and the value used here is 0.25.

The second-difference term in these dissipation models is nonlinear. Its purpose is to introduce an entropy-like condition and to suppress oscillations in the neighborhood of shocks. This term is small in the smooth portion of the flow field. The fourth-difference dissipation term is basically linear and is included to damp high-frequency modes and allow the scheme to approach a steady state. Only this term affects the linear stability of the scheme. Near shocks it is reduced to zero. For high speed flows the switch (10) is not very good and does not allow the multigrid to converge. Instead we consider a TVD variation of the switch [7] given by

$$\nu_{i,j} = \frac{|p_{i+1,j} - 2p_{i,j} + p_{i-1,j}|}{|p_{i+1,j} - p_{i,j}| + |p_{i,j} - p_{i-1,j}| + \epsilon}, \quad \kappa^{(2)} = 1/2. \quad (15)$$

With this change and the factor 1/2 in front of the second-difference dissipation term, the scalar equation becomes first-order upwind near shocks. In the case of the original

ν we find that $\nu \simeq .05$ near shock waves in transonic flows. The parameter ϵ must be chosen carefully to prevent the switch from being activated by noise. In fact we found it useful to take an average of the two versions for ν . Hence, we use

$$\nu_{i,j} = \frac{|p_{i+1,j} - 2p_{i,j} + p_{i-1,j}|}{(1 - \epsilon) * (|p_{i+1,j} - p_{i,j}| + |p_{i,j} - p_{i-1,j}|) + \epsilon * (p_{i+1,j} + 2p_{i,j} + p_{i-1,j})}, \quad (16)$$

with $\epsilon = 1/2$ a reasonable compromise. We now no longer have a free parameter for the second-difference dissipation.

Several other changes were made to the scheme in addition to the change to a TVD switch. In the original algorithm the artificial viscosity for the energy equation was based on the total enthalpy rather than the total internal energy. For high speed flows we base the artificial viscosity on the total internal energy so that in each equation the basic dependent variable is also used in the artificial viscosity. This is more in line with upwind schemes. This has previously been used in central-difference schemes [10]. The algorithm no longer preserves a constant total enthalpy in the steady state (as the Euler equations do), but enthalpy damping is not useful for supersonic flows. In most cases the difference between the two approaches is small with each approach having its advantages. The original form seems to give slightly sharper shocks, while the other one appears to make the scheme more robust.

The form of the dissipation model of the basic or driving scheme is usually modified for coarse grid problems in the multigrid process. A constant coefficient second-difference dissipation is not only less expensive computationally but also generally provides adequate smoothing properties. For high speed flows we find it necessary, as in [4], to append a nonlinear dissipation to the usual one. Here this nonlinear contribution depends on the modified switching function of (16). We also need to increase the constant coefficient from the standard value of $1/16$ to a value of $1/4$.

In order for the scheme to be stable it is necessary to restrict the time step. For transonic flows it is sufficient to base this limitation on the inviscid terms except for extremely fine meshes. For higher speed flows we found it necessary to include a viscous correction to the time step restriction even for crude meshes. We shall thus develop a sufficient condition for stability for the thin-layer equations. Hence, we introduce body fitted coordinates and then ignore all second derivatives except for the $\eta\eta$ derivative. One then obtains the linearized equation

$$W_t + \tilde{A}W_\xi + \tilde{B}W_\eta = \tilde{C}W_{\eta\eta}, \quad (17)$$

where again W is the vector of conserved variables, and the tilde indicates that a matrix is multiplied by the transformation Jacobian J . The matrices of (17) are somewhat complicated. By transforming to nonconservative variables the matrices are greatly simplified, and they have the same eigenvalues. Moreover, W , \tilde{A} , \tilde{B} , and \tilde{C} are replaced by

$$W^* = [\rho \quad u \quad v \quad p]^T, \quad (18)$$

$$A^* = M\tilde{A}M^{-1}, \quad B^* = M\tilde{B}M^{-1}, \quad C^* = M\tilde{C}M^{-1}, \quad (19)$$

where the matrix M is defined according to

$$\frac{\partial W^*}{\partial \alpha} = M \frac{\partial W}{\partial \alpha}, \quad (20)$$

and α is any independent variable. Abarbanel and Gottlieb [11] have shown that one can simultaneously symmetrize all these matrices. They symmetrize the matrices with the similarity transformation determined by

$$S_p = \begin{bmatrix} \frac{\sqrt{\gamma}\rho}{c} & 0 & 0 & 0 \\ 0 & 1 & 0 & 0 \\ 0 & 0 & 1 & 0 \\ \frac{\rho c}{\sqrt{\gamma}} & 0 & 0 & \frac{\sqrt{\gamma-1}}{\sqrt{\gamma}}\rho c \end{bmatrix}, \quad (21)$$

$$S_p^{-1} = \begin{bmatrix} \frac{c}{\sqrt{\gamma}\rho} & 0 & 0 & 0 \\ 0 & 1 & 0 & 0 \\ 0 & 0 & 1 & 0 \\ \frac{-c}{\sqrt{\gamma}\sqrt{\gamma-1}} & 0 & 0 & \frac{\sqrt{\gamma}}{\sqrt{\gamma-1}}\frac{1}{\rho c} \end{bmatrix}. \quad (22)$$

Using this transformation, the triangle inequality, and the condition for symmetric matrices that the spectral radius is equal to the norm, one can easily show that a sufficient stability condition is

$$\frac{1}{\Delta t} \geq \frac{1}{\Delta t_\xi} + \frac{1}{\Delta t_\eta} + \frac{1}{\Delta t_{viscous}} \quad (23)$$

The quantity $1/\Delta t_\xi$ is bounded by the spectral radius of $S_p^{-1}A^*S_p$ given by

$$\bar{\lambda}_\xi = |u\xi_x + v\xi_y| + c\sqrt{\xi_x^2 + \xi_y^2},$$

and similarly the quantity $1/\Delta t_\eta$ is bounded by

$$\bar{\lambda}_\eta = |v\eta_y + u\eta_x| + c\sqrt{\eta_x^2 + \eta_y^2}.$$

The matrix $S_p^{-1}C^*S_p$ is given by

$$\frac{\mu}{3\rho} \begin{bmatrix} 0 & 0 & 0 & 0 \\ 0 & 4\eta_x^2 + 3\eta_y^2 & \eta_x\eta_y & 0 \\ 0 & \eta_x\eta_y & 4\eta_y^2 + 3\eta_x^2 & 0 \\ 0 & 0 & 0 & \frac{3\gamma}{Pr}(\eta_x^2 + \eta_y^2) \end{bmatrix}, \quad (24)$$

and its spectral radius is given by

$$\lambda_{viscous} = \frac{\mu}{3\rho}(\eta_x^2 + \eta_y^2)\max\left[\frac{3\gamma}{Pr}, 4\right].$$

In general the first term in the maximum will be the larger. Hence, we can replace $\lambda_{viscous}$ in (23) by its upper bound. So the actual time step (Δt_{act}) is determined as follows:

$$\Delta t_{act} \leq N \left[\bar{\lambda}_\xi + \bar{\lambda}_\eta + d\frac{\gamma\mu}{Pr\rho}(\eta_x^2 + \eta_y^2) \right]^{-1}, \quad (25)$$

where N is taken to be the allowable CFL number, and the constant d is 4. In the case of steady flows, one can advance the solution at each grid point with the time step determined from this estimate. This type of time stepping provides a preconditioning of

the matrix for the system of difference equations. The preconditioning relaxes stiffness due to variations in local flow properties.

For all flow calculations in this paper a five stage Runge-Kutta scheme with a weighted evaluation, as detailed in [12], of the dissipation terms on the first, third, and fifth stages is used. As described above the time step is reduced in the boundary layer by including the viscous contribution to the time step. In addition, the time step is reduced near shocks by including a term that depends on $\nu_{i,j}$. The reduction is constructed so that there is a CFL number of 1 when $\nu = 1$. It serves to reduce the magnitude of the change in the solution near the shock wave, which exhibits strong nonlinear behavior.

Implicit Residual Smoothing

Implicit residual smoothing of the residuals is used to extend the stability range of the basic time-stepping scheme. For two-dimensional problems, the residual smoothing can be applied in the form

$$(I - \beta_\xi \nabla_\xi \Delta_\xi)(I - \beta_\eta \nabla_\eta \Delta_\eta) \bar{\mathcal{R}}_{i,j}^{(m)} = \mathcal{R}_{i,j}^{(m)}, \quad (26)$$

where the residual $\mathcal{R}_{i,j}^{(m)}$ is defined by

$$\mathcal{R}_{i,j}^{(m)} = \alpha_m \frac{\Delta t_{i,j}}{\Omega_{i,j}} [\mathcal{L}_C W_{i,j}^{(m-1)} + \mathcal{L}_D W_{i,j}^{(0)} - AD^{(m)}] \quad , \quad m = 1, 5 \quad (27)$$

and computed in the Runge-Kutta stage m , and $AD^{(m)}$ is the total artificial dissipation at stage m , and $\bar{\mathcal{R}}_{i,j}^{(m)}$ is the final residual at stage m after the sequence of smoothings in the ξ and η directions. The difference operators \mathcal{L}_C and \mathcal{L}_D are associated with the convection and physical diffusion terms. To derive the maximum stability extension for the hyperbolic problem, the implicit procedure is applied after each stage of the Runge-Kutta scheme. The coefficients β_ξ and β_η are variable and functions of the spectral radii λ_ξ and λ_η . They can be written as follows:

$$\beta_\xi = \max \left\{ \frac{1}{4} \left[\left(\frac{N}{N^*} \frac{1}{1 + \psi r_{\eta\xi}} \right)^2 - 1 \right], 0 \right\}, \quad (28)$$

$$\beta_\eta = \max \left\{ \frac{1}{4} \left[\left(\frac{N}{N^*} \frac{1}{1 + \psi r_{\eta\xi}^{-1}} \right)^2 - 1 \right], 0 \right\},$$

where the ratio $r_{\eta\xi} = \lambda_\eta/\lambda_\xi$, and the quantity N/N^* is the ratio of the CFL number of the smoothed scheme to that of the basic explicit scheme (usually having a value of 2). In hypersonic flow applications we found it necessary for N^* to be 3.25, rather than the value of 3.75 used for transonic computations. From a linear stability analysis, the scheme with these coefficients is stable for all mesh cell aspect ratios when the parameter $\psi \approx .125$ and N/N^* is sufficiently large. The practical limitation on the Courant number is due to the requirement for effective high frequency damping. For large N/N^* the

high frequency damping of the scheme vanishes. The variable coefficients are functions of the local mesh cell aspect ratio, and thus the smoothing process is not activated in a coordinate direction where it is not needed. This is important for best possible convergence. For further discussion of implicit residual smoothing see [13].

Multigrid Method

As indicated earlier the salient features of the multigrid method considered here are fairly standard. Moreover, we apply the Full Approximation Storage (FAS) scheme of Brandt [14] to define the equivalent fine grid problem on a coarse grid. Coarser meshes are obtained by eliminating every other mesh line in each coordinate direction. The grid transfer operators for the solution, residual, and coarse grid corrections are those introduced by Jameson [15]. In particular, on the auxiliary meshes, the solution is initialized as

$$W_{2h}^{(0)} = \frac{\sum \Omega_h W_h}{\Omega_{2h}}, \quad (29)$$

where the subscript refers to the mesh spacing value, the sum is over the four fine grid cells that compose the $2h$ grid cell, and Ω is a cell volume. This rule conserves mass, momentum, and energy. On a coarse grid, a forcing function P is added to the governing discrete equations in order to impose the fine grid approximation. After the initialization of the coarse grid solution, this function is computed as follows:

$$P_{2h} = \sum R_h(W_h) - R_{2h}(W_{2h}^{(0)}), \quad (30)$$

where $R_h(W_h) = \mathcal{L}_h W_h$. Then, the time-stepping scheme on the $(m+1)^{st}$ stage becomes

$$W_{2h}^{(m+1)} = W_{2h}^{(0)} - \alpha_{m+1} \frac{\Delta t}{\Omega} [R_{2h}(W_{2h}^{(m)}) + P_{2h}^{(0)}]. \quad (31)$$

We can also define a new value R^* for the residual as

$$R_{2h}^* = R_{2h}(W_{2h}) + P_{2h}, \quad (32)$$

collect this value, restrict the solution W_{2h} to the next coarser grid, and repeat the process. The corrections computed on a coarse grid are transferred back to a finer grid with bilinear interpolation. In order to execute the multigrid strategy we employ a fixed W-type cycle. To provide a well conditioned starting solution for the fine mesh a Full Multigrid (FMG) method is used. The FMG is analogous to grid sequencing, except multigrid cycles are performed on each coarse grid.

Some of the additional elements of the multigrid method are not necessarily standard. A smoothing of the coarse grid corrections being transferred to the finest grid was found to be beneficial in transonic computations [12]. The smoothing was accomplished with the implicit residual smoothing mentioned previously and a constant coefficient $\beta \approx 0.1$. This smoothing of the residuals on the way to finer meshes is crucial for the convergence of the multigrid for hypersonic flows. Such a process acts to reduce high frequency

oscillations caused by the interpolation. Hence, it becomes especially important near strong shocks, where nonphysical upstream influence can occur. Another important element for high Mach number ($M \geq 10$) flows is the coarse grid correction scheme. That is, the physical viscous terms should also be computed on the coarse meshes.

Boundary Conditions and Initialization

At a solid surface (wall) boundary the no-slip condition is enforced. The wall pressure is set to the value at the first interior solution point, and thus, a reduced normal momentum equation is satisfied. The wall temperature (T_w) is specified. In a finite-volume formulation, this amounts to treating the Cartesian velocity components and the temperature difference $T - T_w$ as antisymmetric functions with respect to the wall. For each of the physical problems considered the Mach number at the inflow boundary exceeds 1.0. Consequently, the dependent variables are specified at this boundary according to the flow conditions. At any outflow boundary, we apply simple extrapolation of the components of the solution vector. In general, for hypersonic flows numerical difficulties are experienced at the start of a calculation if the discrete flow field is initialized with free-stream conditions. To avoid these difficulties we apply the following procedure. The Mach number of the flow is set to a lower value (i.e., 2.0) than the required one. In addition, the wall temperature T_w is set to the free-stream value. Then the Mach number and T_w are gradually increased over a few hundred time steps until the desired flow conditions are obtained. This Mach number ramping is only done on the coarsest mesh in the FMG sequence.

Results

We consider two-dimensional (2-D) hypersonic laminar flow over two different geometries in order to evaluate the present multigrid method. The first geometry is a circular cylinder. For this case the free-stream Mach number (M_∞) is 6.5, and the Reynolds number (Re_D) based on the cylinder diameter D (0.82 meters) is 1.04×10^5 . The free-stream temperature (T_∞) is 202° Kelvin, and the wall temperature is specified at 294° Kelvin. This represents a fairly cold wall condition relative to the temperature after the normal portion of the bow shock. Computed surface pressures and heat transfer rates are compared with the experimental data of Wieting [16]. The second geometry is the 15 degree compression ramp tested by Holden and Moselle [17]. For this flow problem the free-stream Mach number is 14.1, and the Reynolds number based on a reference length L (0.44 meters) is 1.04×10^5 . The length of the flat plate preceding the ramp is L . The T_∞ is 89° Kelvin, and the wall temperature is 296° Kelvin. Surface distributions of pressure coefficient (c_p), skin-friction coefficient (c_f), and heat transfer coefficient (c_h) calculated with the present multigrid method are compared with experimental data of [17]. These coefficients have the standard definitions. In all calculations for both cases we assume that the working fluid (air) is thermally and calorically perfect. Sutherland's law is used to determine the molecular viscosity.

Cylinder Flow

The 2-D cylinder flow was computed on a 64×64 grid and a 128×128 grid. In figure 1 the 64×64 grid, which is a proper subset of the 128×128 grid, is shown. For both grids the circumferential spacing is uniform. In the normal direction on the

centerline, the mesh is clustered at the surface with minimum spacings of approximately $4 \times 10^{-4} D$ and $2 \times 10^{-4} D$ for the two meshes. At the circumferential angle (θ) of -90 degrees or +90 degrees, the normal mesh spacings are increased by nearly 60 percent of the centerline values. This was done to accommodate the boundary-layer growth as well as the resolution of the inviscid flow region. As evident from figure 2, the normal spacing through the shock region is uniform. Convergence histories, which define the variation of the error with multigrid cycles, corresponding to both grids are displayed in figure 3. The error is measured as an rms value of the residual for the continuity equation. In figure 3 one observes three out of the four levels of refinement in the FMG procedure. The first level, which requires only a couple of CPU seconds, is used for the initialization (Mach number ramping), and thus it is not shown. There are three grids on both the third and the fourth levels. On the 128×128 mesh the residual is reduced nearly 6 orders of magnitude in 300 cycles. This requires about 5 minutes of CPU time on a Cray YMP. It should be emphasized that for engineering accuracy (i.e., residual reduced by 3 orders) the finest mesh calculation required about 2 minutes. Note that when engineering accuracy is achieved, there is no appreciable improvement in the viscous solution accuracy by further residual reduction.

In figure 4 the computed surface distributions of pressure and heat transfer rate are presented. There is very good agreement between the predictions with the 128×128 grid and the experimental data. For the 64×64 grid the scaled heat transfer rate (Q/Q_{ref}) is overpredicted for $\theta < -25$ degrees and $\theta > +25$ degrees. This indicates that opening the normal mesh spacing adjacent to the surface produced a spacing too large for the 64×64 grid, when only a first-order approximation is used for the temperature derivative. The Mach number and pressure contours for the two calculations are shown in figures 5 and 6, respectively. The smoothness of the contours is evident, and the improved shock resolution with mesh refinement is readily seen. In addition, one can notice that the boundary layer is extremely thin for this case.

Compression Ramp Flow

The 2-D compression ramp flow was computed on grids consisting of 56×64 (number of streamwise cells \times number of normal cells) and 112×128 cells. Figure 7 depicts the 56×64 grid. There is streamwise clustering at the leading edge of the flat plate and at the start of 15 degree ramp. The minimum spacing is approximately $5.8 \times 10^{-3} L$. Again, to resolve the boundary layer, the mesh is clustered in the normal direction near the surface. The normal spacings for the coarse and fine grids are about $4.6 \times 10^{-4} L$ and $2.3 \times 10^{-4} L$, respectively. In figure 8 the convergence histories for this case with the scalar and matrix forms of the dissipation model are presented. The convergence rates with both forms are quite good on the 56×64 grid, allowing the residual to be decreased about 6 orders of magnitude in 300 cycles. The average rate of reduction of the residual with the scalar model (0.954) is slightly faster. There is some deterioration in the rates with mesh refinement. This slowdown with mesh refinement is also observed for transonic computations. Although the average rates of residual decay using the two dissipation forms is essentially the same (0.965), the asymptotic rate is faster using the scalar model. The residual is reduced just about 5 orders in 300 multigrid cycles with the scalar formulation. It should be pointed out that in the multigrid calculation with the scalar model four grids were applied. Only three grids were used in conjunction with the matrix model, due to numerical difficulties caused by the sudden switch from

free-stream conditions to a wall bounded flow at the inflow boundary.

To provide a better understanding of the computed results for this compression ramp case, we will first describe the physics of the flow. Due to the development of the boundary layer on the flat plate, the inviscid flow is turned, and an oblique shock wave is produced. Compression waves are formed by the turning of the flow at the start of the compression ramp. These waves coalesce to form another oblique shock. The shock wave emanating from the leading edge of the plate intersects the compression ramp shock. It needs to be emphasized that accurate predictions of this flow field depend strongly on a good resolution of the leading edge shock. Also, resolution of the boundary layer on the ramp is demanding. There is a substantial thinning of the boundary layer on the ramp as a consequence of the flow being compressed.

In figures 9-11 comparisons are made between the computed variations of the pressure, skin-friction, and heat transfer coefficients and the corresponding experimental data. To further assess the shock capturing capability of the present central-difference scheme, results calculated with the code developed by J. L. Thomas, which is based on the Riemann solver of Roe and described in [18], are also included in these figures. The computed distributions exhibit excellent agreement with the data in nearly all cases. With the scalar dissipation model, there are differences between the solutions on the 56 x 64 grid and the 112 x 128 grid. The results obtained using the matrix model for these two grids almost coincide. Moreover, the solution computed with the matrix model on a 56 x 64 mesh is comparable to the one calculated with the scalar formulation on a 112 x 128 mesh. Figures 12 and 13 show the pressure contours on the ramp for each of the present computations. One can clearly see the effects of dissipation and mesh size on the leading edge shock and the interaction region of the two shocks.

Concluding Remarks

A multigrid method with central differencing has been successfully applied to the solution of hypersonic viscous flows. An explicit five stage Runge-Kutta scheme has been used as a smoother in solving the time-dependent, thin-layer Navier-Stokes equations. In this paper considerable emphasis has been focussed on the dissipative characteristics of the driving scheme for the multigrid process. The presence of strong shocks has required the introduction of a switching function for the numerical dissipation based on TVD principles. In addition, as a consequence of the strong shocks, a nonlinear coefficient, which is dependent on this switching function, has been included in the coarse grid dissipation formulation. This nonlinear coefficient is not needed for transonic computations. We have also considered both scalar and matrix forms of the dissipation model.

Numerical solutions have been obtained for hypersonic laminar flow over a 2-D cylinder and a 2-D compression ramp. The agreement between predictions and experimental data is quite good. Engineering accuracy has been obtained rapidly in all computations, requiring about 2 CPU minutes on the Cray YMP.

Acknowledgement

The authors would like to express their appreciation to Dr. J. L. Thomas of NASA Langley Research Center for providing numerical results obtained with the upwind scheme of Roe.

References

- [1] Jameson, A. and Baker, T. J., *Multigrid Solution of the Euler Equations for Aircraft Configurations*, AIAA Paper 84-0093, Jan. 1984.
- [2] Radespiel, R., Rossow C., and Swanson, R. C., *An Efficient Cell-Vertex Multigrid Scheme for the Three-Dimensional Navier-Stokes Equations*, AIAA Paper 89-1953, June 1989.
- [3] Vatsa, V. N. and Wedan, B. W., *Development of an Efficient Multigrid Code for 3-D Navier-Stokes Equations*, AIAA Paper 89-1791, June 1989.
- [4] Kroll, N., Radespiel, R., and Rossow C.-C., *Experiences with Explicit Time-Stepping Schemes for Supersonic Flow Fields*, Proceedings of Eighth GAMM Conference on Numerical Methods in Fluid Dynamics, Delft, The Netherlands, Sept. 27-29, 1989.
- [5] Radespiel, R. and Kroll, N., *A Multigrid Scheme with Semicoarsening for Accurate Computations of Viscous Flows*, 12th International Conference on Numerical Methods in Fluid Dynamics, University of Oxford, July 1990.
- [6] Jameson, A., Schmidt, W., and Turkel, E., *Numerical Solutions of the Euler Equations by Finite Volume Methods Using Runge-Kutta Time-Stepping Schemes*, AIAA Paper 81-1259, June 1981.
- [7] Swanson, R. C. and Turkel, E., *On Central-Difference and Upwind Schemes*, ICASE Report 90-44, 1990, submitted to Journal of Comput. Physics.
- [8] Pulliam, T. H., *Artificial Dissipation for the Euler Equations*, AIAA Journal, Vol.24, 1986, pp. 1931-1940.
- [9] Jameson, A. and Yoon, S., *Lower-Upper Implicit Schemes with Multiple Grids for the Euler Equations*, AIAA Journal, Vol. 25, 1987, pp. 929-935.
- [10] Caughey, D. A. and Turkel, E., *Effects of Numerical Dissipation on Finite-Volume Solutions to Compressible Flow Problems*, AIAA Paper 88-0621, Jan. 1988.
- [11] Abarbanel, S. and Gottlieb, D., *Optimal Time Splitting for Two- and Three-Dimensional Navier-Stokes Equations with Mixed derivatives*, J. Comput. Physics, Vol. 41, 1981, pp. 1-33.
- [12] Swanson, R. C. and Radespiel, R., *Cell Centered and Cell Vertex Multigrid Schemes for the Navier-Stokes Equations*, AIAA Journal, Vol. 29, 1991, pp. 697-703.
- [13] Swanson, R. C. and Turkel, E., *Multistage Schemes with Multigrid for the Euler and Navier-Stokes Equations*, NASA Technical Paper, 1991 (to be published).
- [14] Brandt, A., *Multi-Level Adaptive Solutions to Boundary-Value Problems*, Vol. 31, No. 138, April 1977, pp. 333-390.
- [15] Jameson, A., *Multigrid Algorithms for Compressible Flow Calculations*, MAE Report 1743, Princeton University, Text of lecture given at 2nd European Conference on Multigrid Methods, Cologne, Oct. 1985.

- [16] Wieting, A. R., *Experimental Study of Shock Wave Interference Heating on a Cylindrical Leading Edge*, NASA TM 100484, May 1987.
- [17] Holden, M. S. and Moselle, J. R., *Theoretical and Experimental Studies of the Shock Wave-Boundary Layer Interaction on Compression Surfaces in Hypersonic Flow*, ARL 70-0002, Jan. 1970.
- [18] Vatsa, V. N., Thomas, J. L., and Wedan, B. W., *Navier-Stokes Computations of Prolate Spheroids at Angle of Attack*, AIAA Paper 87-2627, Aug. 1987.

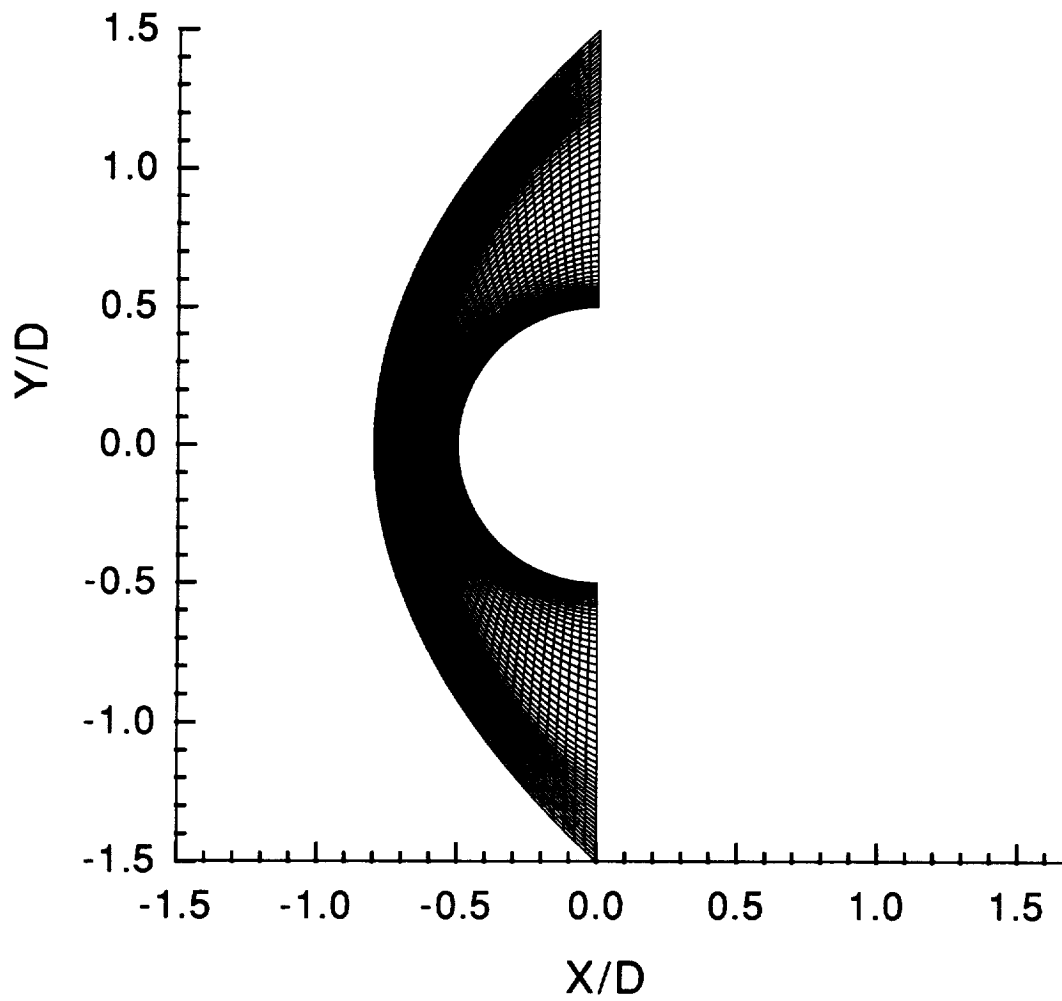


Figure 1 A 64 x 64 grid for 2-D cylinder flow

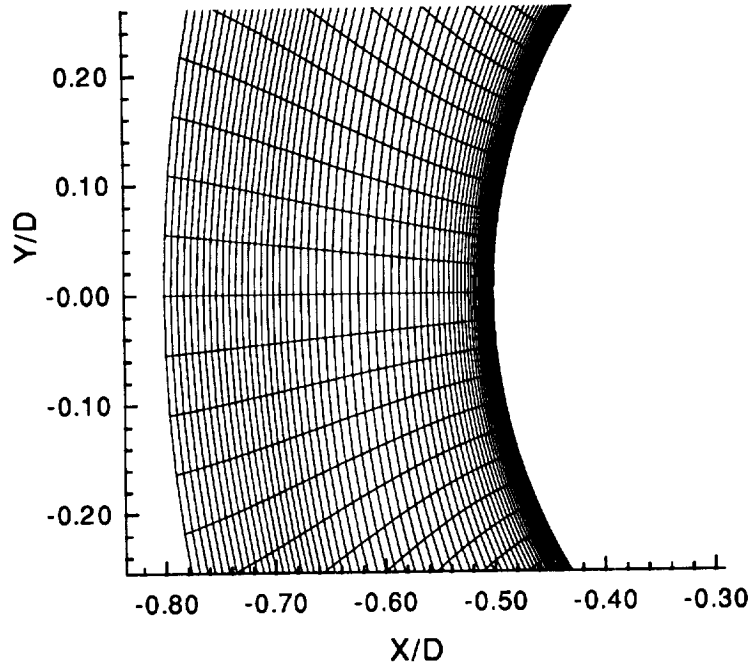


Figure 2 Blowup of 64 x 64 grid for 2-D cylinder flow

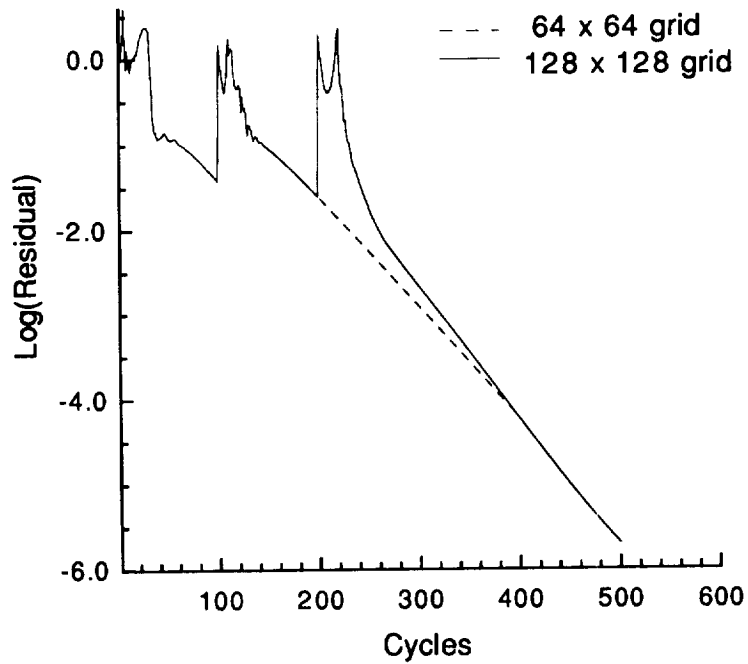
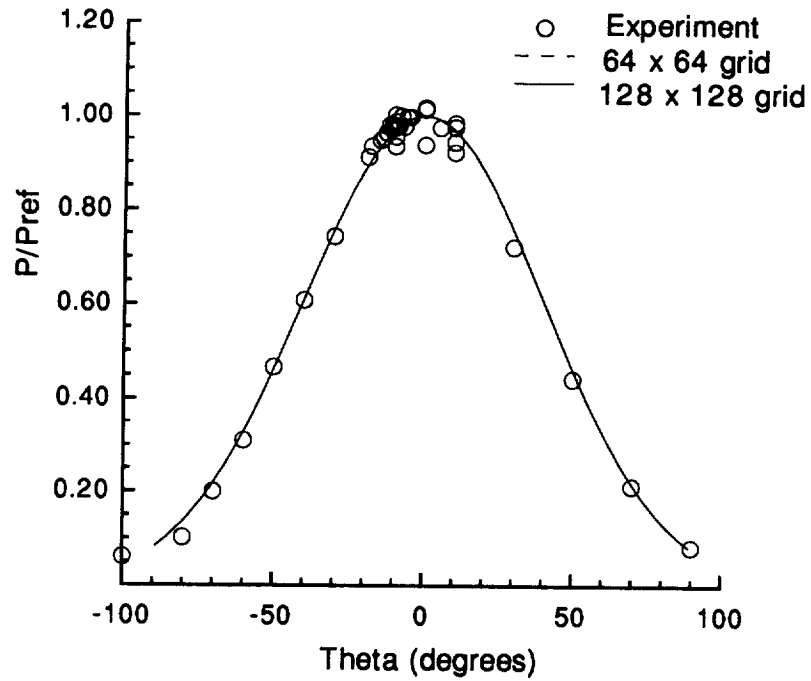
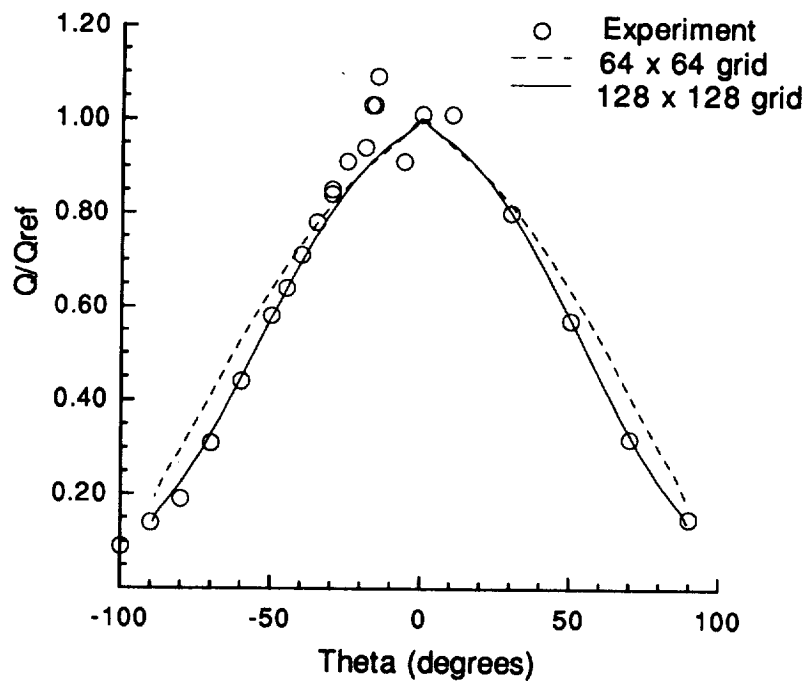


Figure 3 Convergence histories for 2-D cylinder flow computations ($M_\infty = 6.5$, $\alpha = 0.0$ deg, $Re_D = 1.04 \times 10^5$)

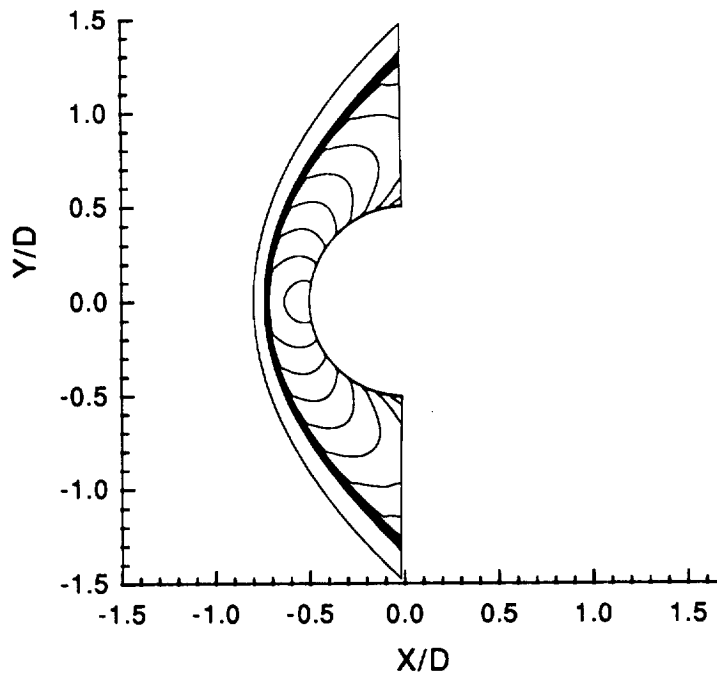


(a) Pressure distribution

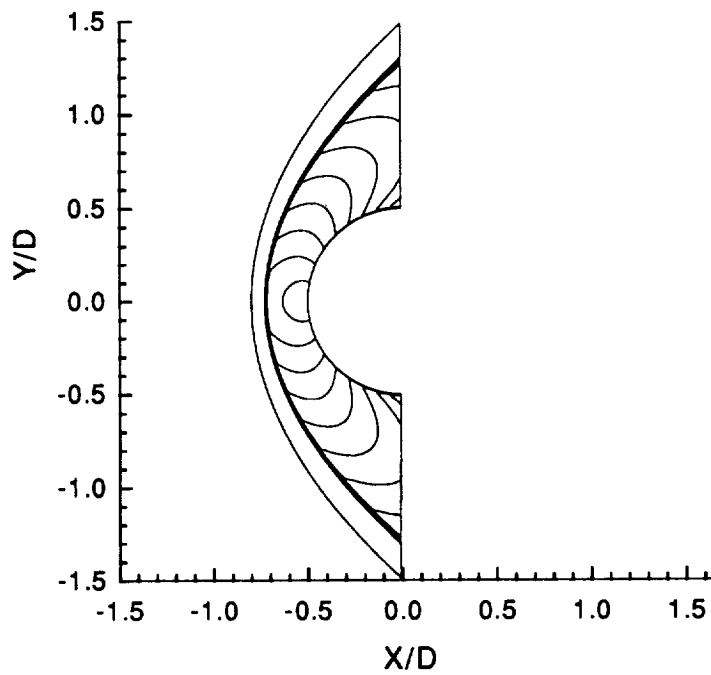


(b) Heat transfer rate distribution

Figure 4 Surface distributions of pressure and heat transfer rate for 2-D cylinder flow ($M_\infty = 6.5$, $\alpha = 0.0$ deg, $Re_D = 1.04 \times 10^5$)

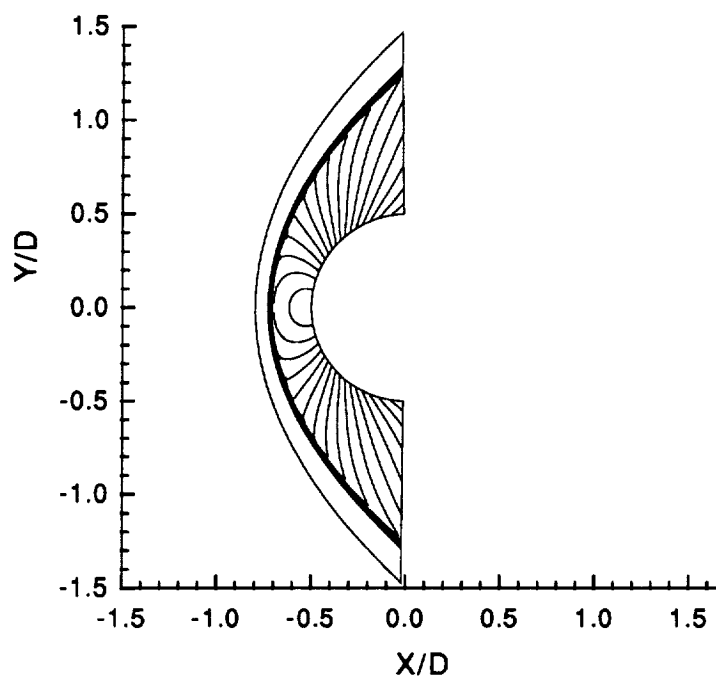


(a) 64 x 64 grid

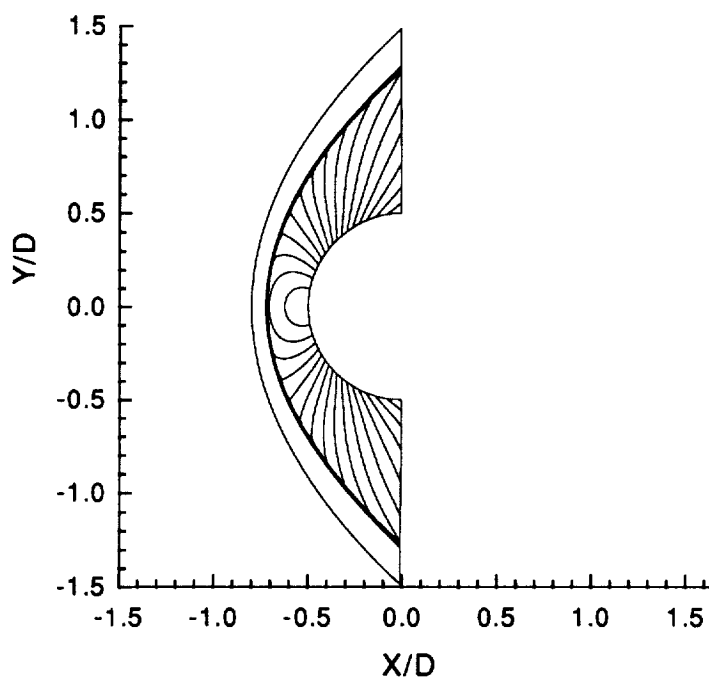


(b) 128 x 128 grid

Figure 5 Mach number contours, with $\Delta M = 0.25$, for 2-D cylinder flow ($M_\infty = 6.5$, $\alpha = 0.0$ deg, $Re_D = 1.04 \times 10^5$)



(a) 64 x 64 grid



(b) 128 x 128 grid

Figure 6 Pressure contours for 2-D cylinder flow
 ($M_\infty = 6.5$, $\alpha = 0.0$ deg, $Re_D = 1.04 \times 10^5$)

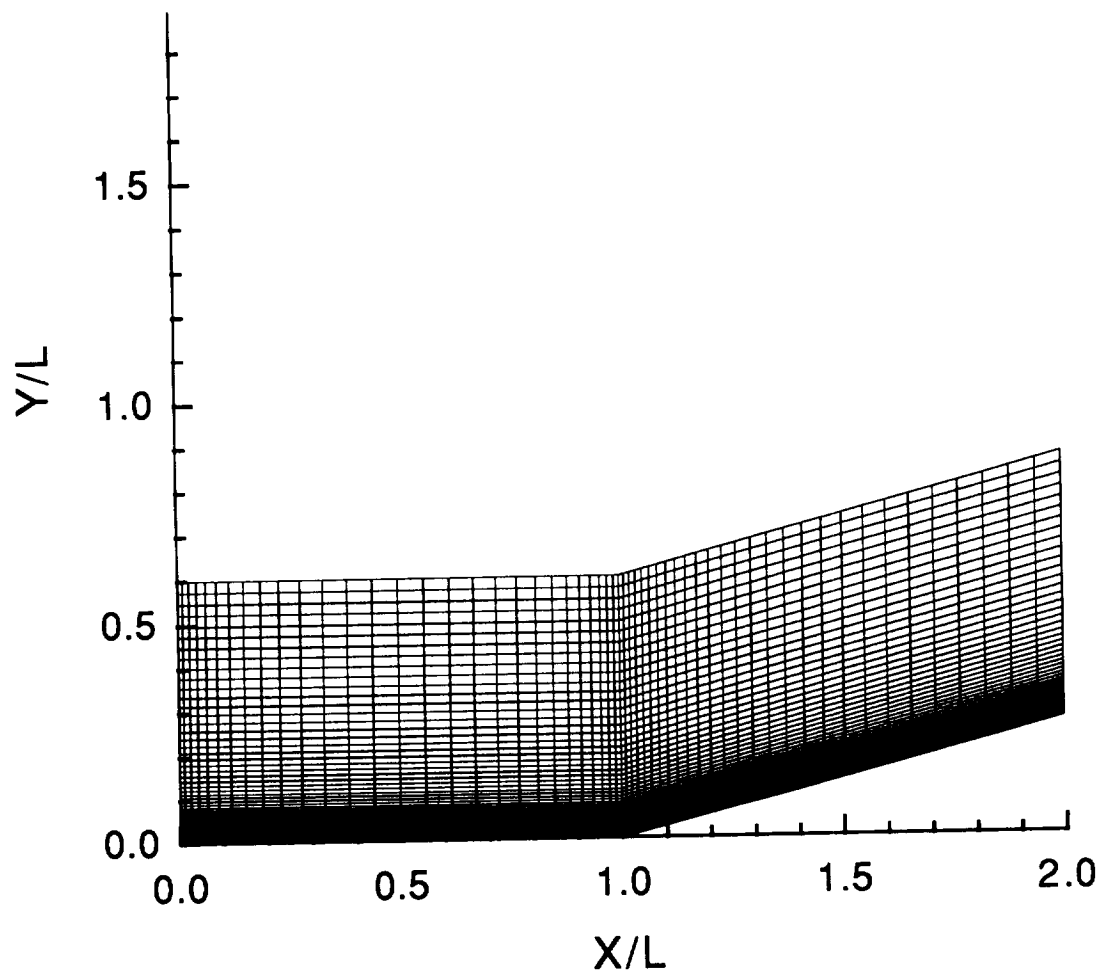
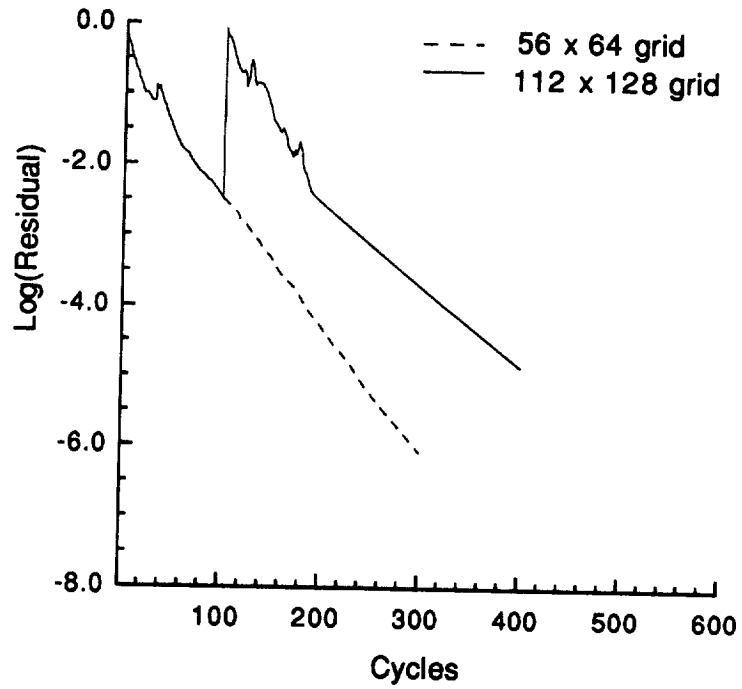
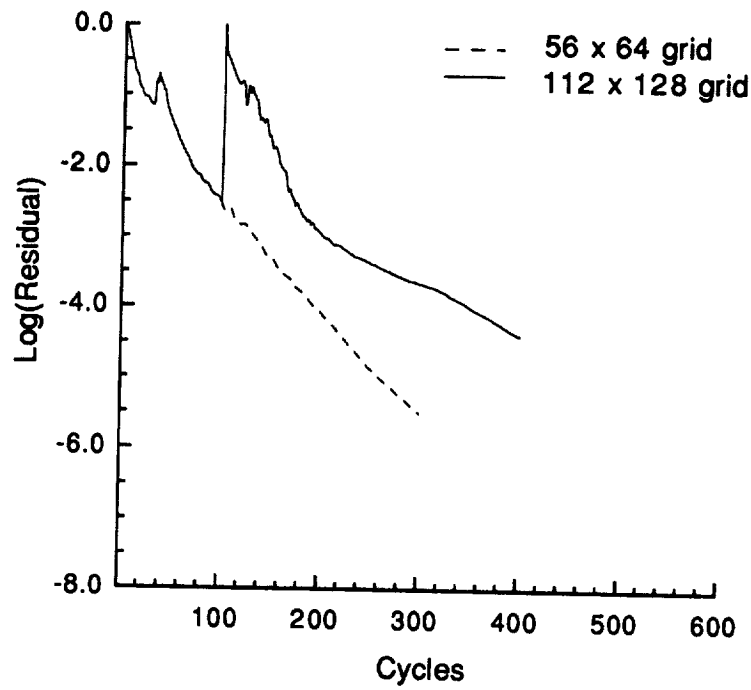


Figure 7 A 56 x 64 grid for 2-D compression ramp flow

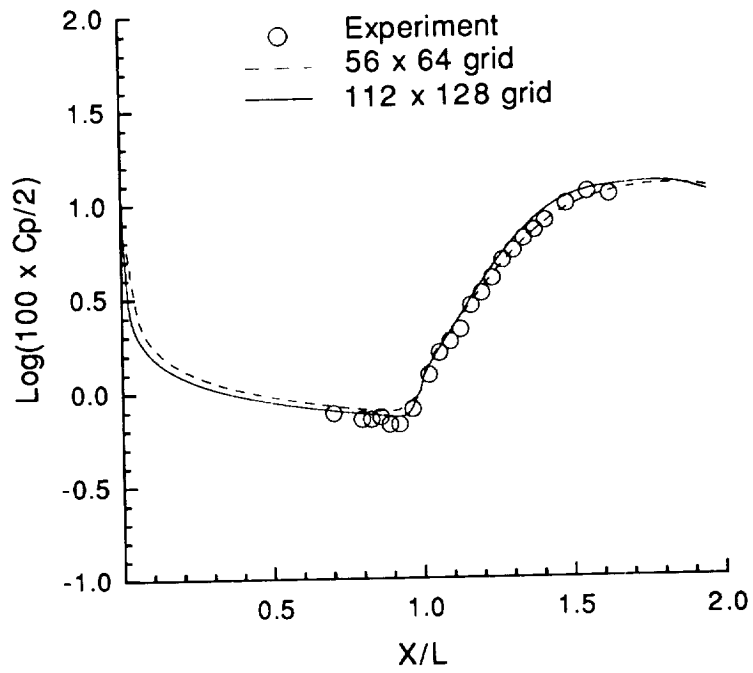


(a) Scalar dissipation

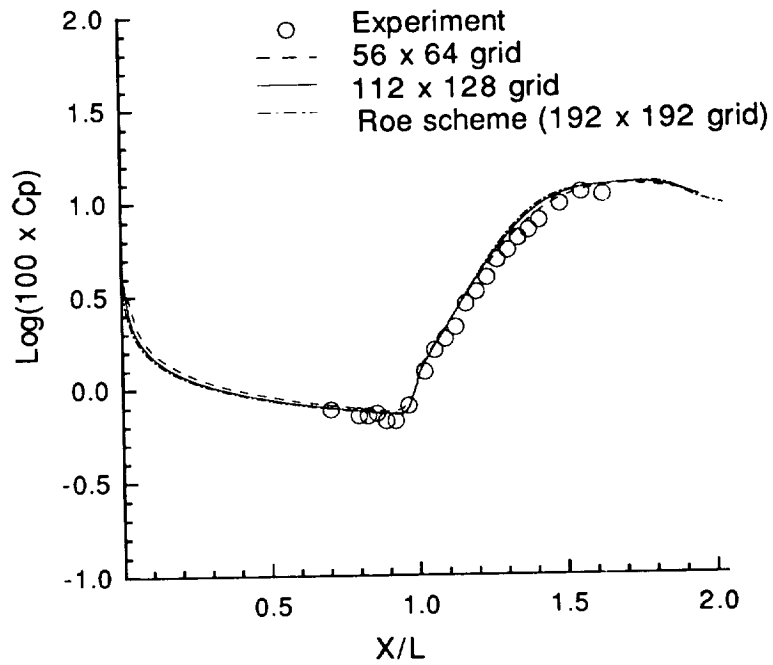


(b) Matrix dissipation

Figure 8 Convergence histories for 2-D compression ramp flow ($M_\infty = 14.1$, $Re_L = 1.04 \times 10^5$, 15 degree ramp)

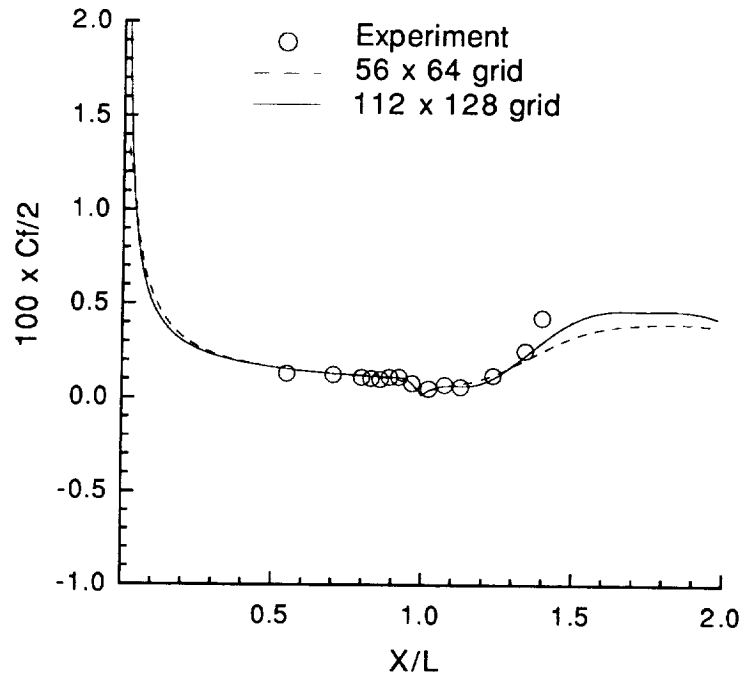


(a) Scalar dissipation

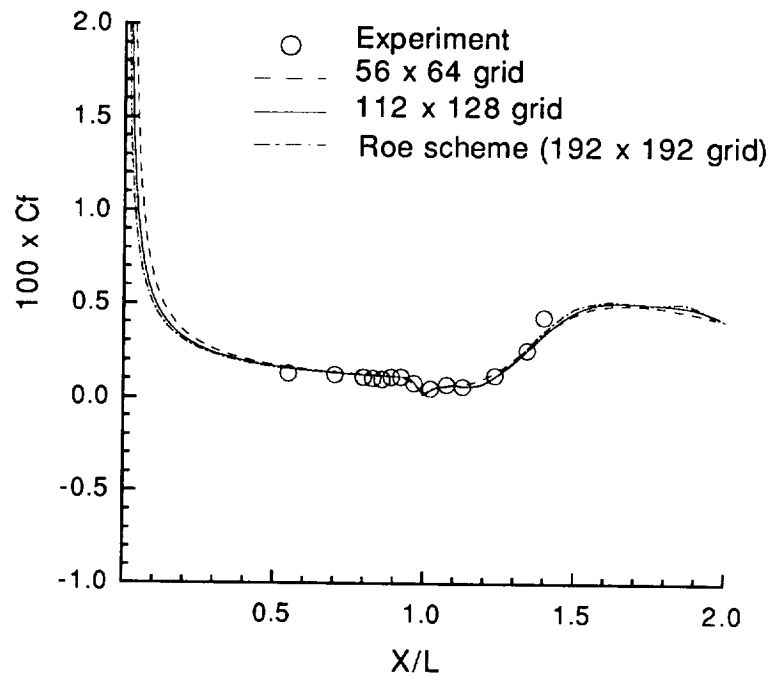


(b) Matrix dissipation

Figure 9 Pressure coefficient distributions for 2-D compression ramp flow ($M_\infty = 14.1$, $Re_L = 1.04 \times 10^5$, 15 degree ramp)

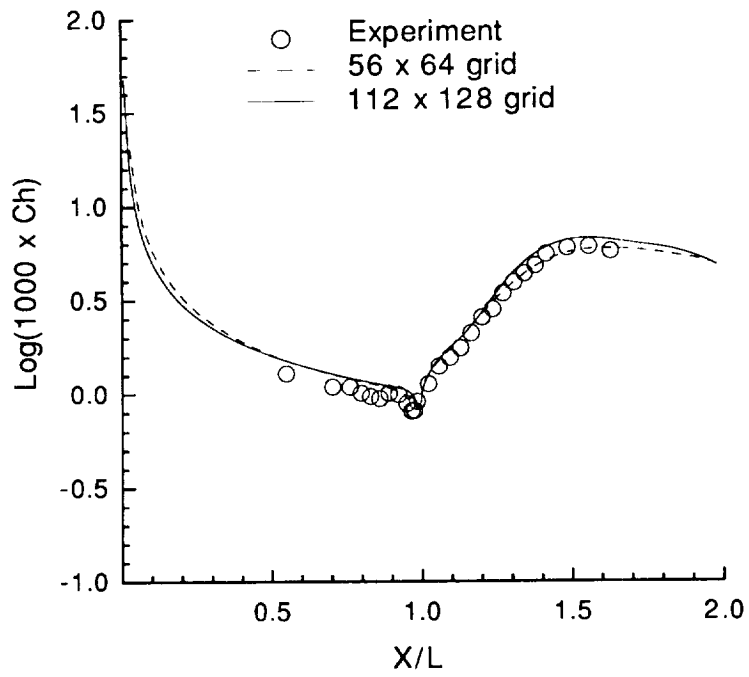


(a) Scalar dissipation

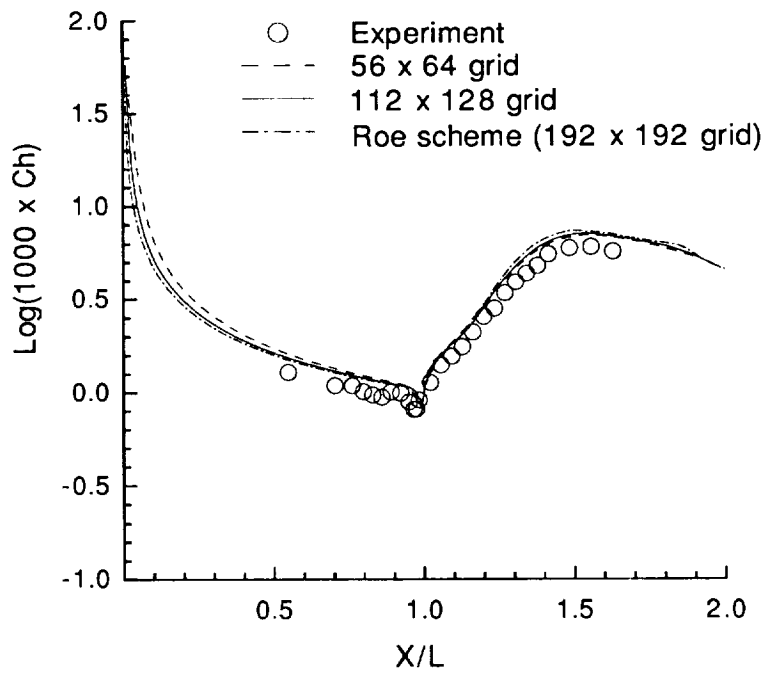


(b) Matrix dissipation

Figure 10 Skin-friction coefficient distributions for 2-D compression ramp flow ($M_\infty = 14.1$, $Re_L = 1.04 \times 10^5$, 15 degree ramp)

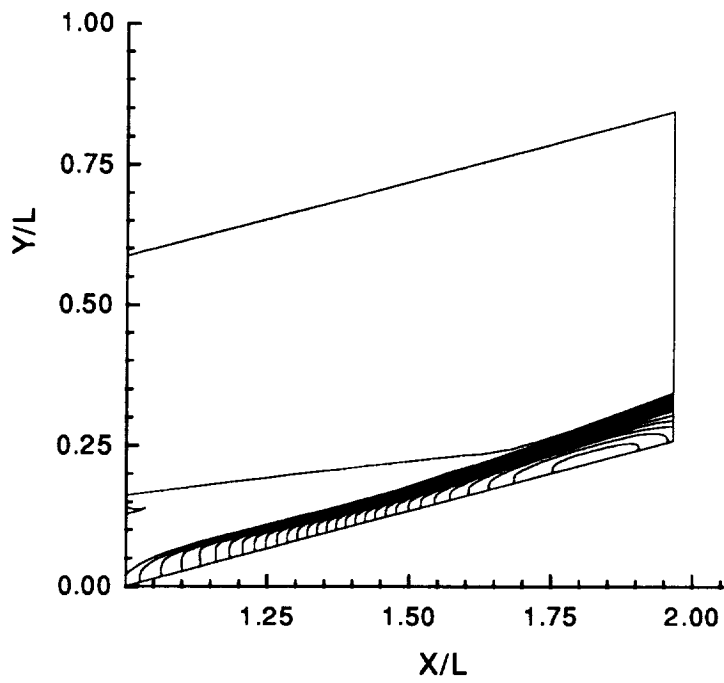


(a) Scalar dissipation

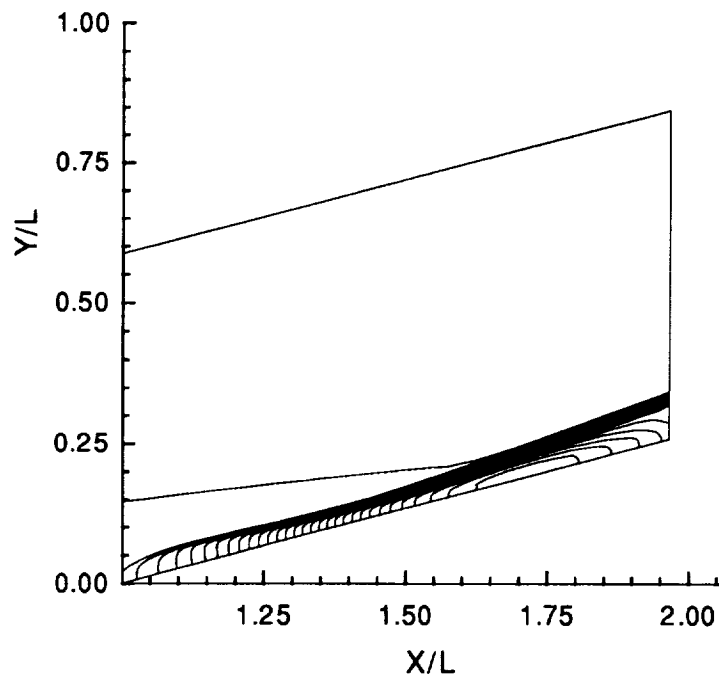


(b) Matrix dissipation

Figure 11 Heat transfer coefficient distributions for 2-D compression ramp flow ($M_\infty = 14.1$, $Re_L = 1.04 \times 10^5$, 15 degree ramp)

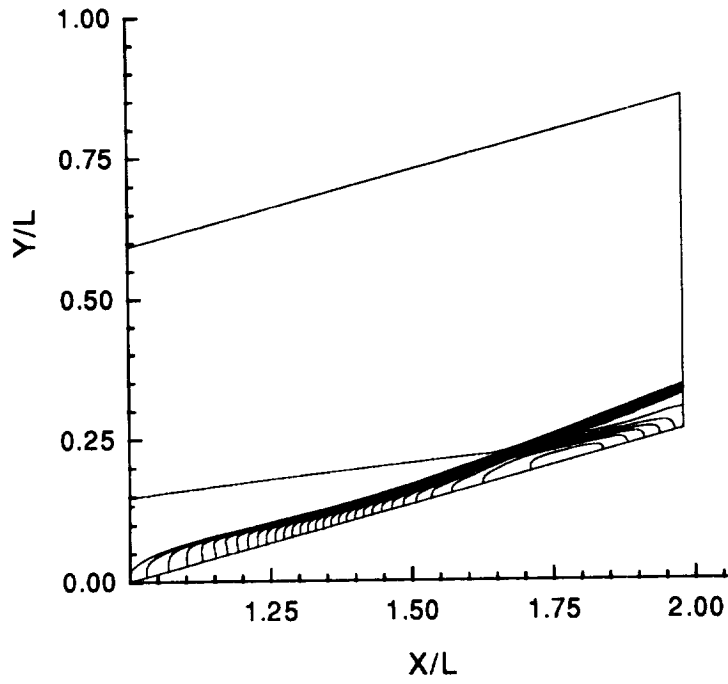


(a) Scalar dissipation

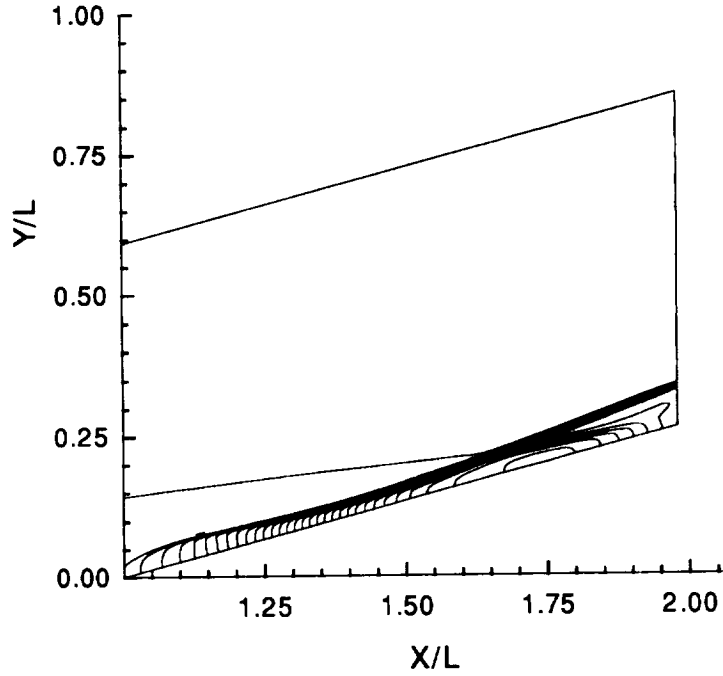


(b) Matrix dissipation

Figure 12 Pressure contours for 2-D compression ramp flow on 56 x 64 grid ($M_\infty = 14.1$, $Re_L = 1.04 \times 10^5$, 15 degree ramp)



(a) Scalar dissipation



(b) Matrix dissipation

Figure 13 Pressure contours for 2-D compression ramp flow on 112 x 128 grid ($M_\infty = 14.1$, $Re_L = 1.04 \times 10^5$, 15 degree ramp)



Report Documentation Page

1. Report No. NASA CR-187602 ICASE Report No. 91-56		2. Government Accession No.		3. Recipient's Catalog No.	
4. Title and Subtitle AN EFFECTIVE MULTIGRID METHOD FOR HIGH-SPEED FLWOS				5. Report Date July 1991	
				6. Performing Organization Code	
7. Author(s) R. C. Swanson E. Turkel J. A. White				8. Performing Organization Report No. 91-56	
				10. Work Unit No. 505-90-52-01	
9. Performing Organization Name and Address Institute for Computer Applications in Science and Engineering Mail Stop 132C, NASA Langley Research Center Hampton, VA 23665-5225				11. Contract or Grant No. NAS1-18605	
				13. Type of Report and Period Covered Contractor Report	
12. Sponsoring Agency Name and Address National Aeronautics and Space Administration Langley Research Center Hampton, VA 23665-5225				14. Sponsoring Agency Code	
				15. Supplementary Notes Langley Technical Monitor: Michael F. Card Submitted to Journal of Communications in Applied Numerical Methods Final Report	
16. Abstract We consider the use of a multigrid method with central differencing to solve the Navier-Stokes equations for high-speed flows. The time-dependent form of the equations is integrated with a Runge-Kutta scheme accelerated by local time stepping and variable coefficient implicit residual smoothing. Of particular importance are the details of the numerical dissipation formulation, especially the switch between the second and fourth difference terms. Solutions are given for two-dimensional laminar flow over a circular cylinder and a 15 degree compression ramp.					
17. Key Words (Suggested by Author(s)) multigrid, hypersonics, Navier-Stokes			18. Distribution Statement 02 - Aerodynamics 64 - Numerical Analysis Unclassified - Unlimited		
19. Security Classif. (of this report) Unclassified		20. Security Classif. (of this page) Unclassified		21. No. of pages 27	22. Price A03